npj | climate and atmospheric science

Article

Published in partnership with CECCR at King Abdulaziz University

https://doi.org/10.1038/s41612-025-01201-x

Tropical volcanic impacts on MENA climate via ENSO and NAO dynamics in a high-top model

Muhammad Mubashar Dogar[1,2] ✉, Shingo Watanabe[1,3], Masatomo Fujiwara[4], Muhammad Adnan Abid[5,6], Turki M. Habeebullah[7] & Basit Khan[8]

Volcanic eruptions are among the strongest climate drivers, yet their regional impacts on the Middle East and North Africa (MENA) remain poorly constrained. Post-eruption amplified winter cooling in MENA is often attributed to a volcanically forced positive North Atlantic Oscillation (NAO), but the concurrent occurrence of El Niño–Southern Oscillation (ENSO) complicates attribution. Furthermore, summer climatic responses, including tropical warming and mid-latitude cooling, remain underexplored. Here, we present a pioneering research using a high-top coupled climate model (MIROC6) to assess volcanic-induced ENSO–NAO interactions and their regional climate impacts. We demonstrate that volcanic-induced NAO variability is the primary driver of post-eruption MENA winter cooling, with El Niño acting as a modulator rather than a fundamental trigger. We further reveal distinct summer climate anomalies, including suppressed precipitation over the Intertropical Convergence Zone (ITCZ). These findings underscore the importance of high-top models to resolve stratospheric influences on post-volcanic climate variability.

Volcanic eruptions are a major external climate forcing, injecting sulfur dioxide into the stratosphere, where it forms aerosols that reflect solar radiation, leading to global cooling[1–3]. While these global effects are well-documented[1,4], their influence on large-scale atmospheric circulation patterns, particularly the El Niño-Southern Oscillation (ENSO) and North Atlantic Oscillation (NAO), remains debated[3–6]. This is especially true for the Middle East and North Africa (MENA), where the interplay between volcanic aerosols, atmospheric circulation, and regional climate responses is complex[7,8–12].

Large tropical eruptions are often associated with a positive NAO phase, which induces Eurasian warming and MENA cooling, as observed after the El Chichón (1982) and Pinatubo (1991) eruptions[7,11,13]. However, some studies argue that high-latitude winter warming may be driven more by internal climate variability—such as ENSO or intrinsic NAO fluctuations—rather than by a volcanic-induced NAO response[5,6,14–16]. Others suggest that an El Niño-like pattern is necessary to trigger a positive NAO phase[14], while some reconstructions question the robustness of these links[6]. Recent findings[11] highlight volcanic-induced NAO as a key driver of Eurasian warming, whereas El Niño-like variability explains warming in the Americas, challenging the necessity of ENSO preconditioning. However, these conclusions were drawn using low-top models, necessitating further investigation with high-top coupled models.

MENA (5°S–45°N, 20°W–70°E) is highly vulnerable to climate variability, with critical socio-economic implications for water resources and agriculture[7,17–20]. Historical eruptions have caused significant regional disruptions in MENA, including crop failures[18,21]. The 1991 Pinatubo eruption led to unusually cold winters and even snowfall in parts of the Arabian Peninsula[1,7,12]. Despite substantial research on volcanic impacts at high latitudes, less attention has been given to post-eruption cooling anomalies in MENA.

This study investigates how tropical volcanic eruptions influence the MENA climate by modulating the polar vortex and NAO. Volcanic aerosols induce stratospheric warming primarily between 30°S and 30°N, strengthening the meridional temperature gradient and intensifying the polar vortex, which in turn influences NAO variability[1,9,22–24]. While some emphasize ENSO's role in shaping post-volcanic patterns[5,14], others suggest volcanic

[1]Research Center for Environmental Modeling and Application (CEMA), Japan Agency for Marine-Earth Science and Technology (JAMSTEC), Yokohama, Japan. [2]Global Change Impact Studies Centre (GCISC), Ministry of Climate Change (MoCC), Islamabad, Pakistan. [3]Advanced Institute for Marine Ecosystem Change (WPI-AIMEC), Tohoku University, Sendai, Japan. [4]Faculty of Environmental Earth Science, Hokkaido University, Sapporo, Japan. [5]Atmospheric, Oceanic and Planetary Physics, Department of Physics, University of Oxford, Oxford, UK. [6]National Centre for Atmospheric Science (NCAS), Oxford, UK. [7]National Center for Meteorology, Jeddah, Saudi Arabia. [8]Mubadala Arabian Center for Climate and Environmental Sciences, New York University Abu Dhabi, Abu Dhabi, United Arab Emirates. ✉e-mail: mubashardogar@yahoo.com; dogarm@jamstec.go.jp

activity can independently drive these processes[5,14]. Understanding these interactions is crucial for predicting climate responses and informing adaptation strategies.

Previous studies have primarily used models with limited vertical resolution[25–32], which may struggle to resolve key stratospheric processes such as post-eruption polar vortex intensification and NAO variability[10,33]. Khodri et al.[26] demonstrated that tropical eruptions can trigger El Niño by cooling tropical Africa, while Luo et al.[34] showed ENSO-driven NAO phase shifts, highlighting unresolved volcanic–ENSO–NAO interactions. These limitations—in both vertical model resolution and representation of interlinked dynamical processes—underscore the need for high-top models like MIROC6. MIROC6 extends up to 0.004 hPa with 90 vertical levels, providing a more complete and physically consistent simulation of stratosphere–troposphere coupling and associated teleconnections.

To address the above limitations in model vertical resolution and the representation of volcanic–ENSO–NAO interactions, we use MIROC6 to explore ENSO and NAO responses to volcanic forcing, with a focus on post-eruption MENA cooling. Specifically, we aim to answer:

How well does MIROC6 simulate the climatic impacts of volcanic eruptions on MENA, particularly through ENSO–NAO interactions?

What drives post-eruption amplified winter cooling and summer climatic shifts—NAO or ENSO?

How does ENSO preconditioning (El Niño, La Niña, or neutral) modulate the magnitude and spatial pattern of post-eruption climate responses in MENA?

To reinforce the robustness of our findings, we compare our idealized simulations with independent datasets, including observational (UDEL), reanalysis (ERA5), and CMIP6 multi-model ensemble outputs (section "Comparison with observations, reanalysis, and CMIP6 models"). The subsequent sections present our results, including model validation against ERA5 reanalysis (section "Model evaluation and variability"), key findings on ENSO–NAO responses to strong volcanism, and broader implications (section "Discussion"). The experimental design and methodology are described in the section "Methods."

Results

Model evaluation and variability

The post-eruption low-latitude winter cooling, particularly over MENA, is a key focus of this study. To validate the MIROC6 model's performance, we analyze its climatological patterns during boreal winter, comparing them with ERA5 reanalysis data[35,36].

Figure 1 presents the MIROC6 global climatology for boreal winter (DJF), providing a reference for large-scale circulation patterns that influence the MENA region. Figure 1 presents the MIROC6 global climatology for boreal winter (DJF), compared against ERA5, showing surface air temperature, precipitation, and 10 m wind vectors. While the figure provides a global overview, it offers important context for evaluating large-scale circulation features—such as the NAO and ENSO—that influence regional climate variability over MENA. Winter climatology is prioritized due to the stronger indirect circulation effects driven by ENSO and NAO variability, making it an optimal season for assessing model responses.

To further evaluate the model's baseline performance, we computed DJF climatological differences between MIROC6 and ERA5 for surface air temperature, precipitation, and 10 m wind vectors (Supplementary Fig. S2). The MIROC6 control simulation, conducted with fixed forcings (held constant at 1991 levels) and using hypothetical model years, was compared against ERA5 over the 1941–2002 period to ensure consistent sampling. Given that ERA5 incorporates transient forcings (e.g., greenhouse gases, volcanic aerosols) and assimilated observations, the differences likely reflect a combination of model bias, forcing discrepancies, and internal variability. MIROC6 generally reproduces large-scale temperature patterns, with small biases in the tropics and mid-latitudes, and a persistent warm bias at high latitudes, especially over North America. Over the MENA region, temperature and precipitation differences are modest, though localized precipitation biases appear in tropical regions such as Southeast Asia and South America—possibly linked to convection schemes and the lack of transient forcings. Wind differences are relatively minor and spatially coherent. Overall, the comparison confirms the model's broad reliability, while highlighting regional deviations important for interpreting post-volcanic and dynamical responses over MENA.

To establish MIROC6's capability in capturing large-scale climate patterns, we evaluate its simulation of NAO- and ENSO-related temperature and pressure shifts (Figs. S3 and S4). The strong correlation between MIROC6 and ERA5 climatology confirms that the model effectively simulates the positive NAO phase, characterized by a high-pressure anomaly over the Azores extending toward North Africa and a low-pressure anomaly over northern latitudes[7,37,38].

Surface temperature anomalies associated with the positive NAO phase exhibit warming over Eurasia and cooling over MENA, consistent with earlier findings. While the MIROC6 simulation shows weaker warming over the southeastern United States than observed in ERA5, the overall spatial pattern aligns well with observational datasets, confirming MIROC6's robustness in simulating the NAO response. The model's effectiveness is further supported by the correlation of the Niño3.4 index with surface temperature (Fig. S4).

Post-volcanic MENA winter response—influence of ENSO and NAO dynamics

Figure 2a–c presents surface temperature anomalies during the first post-eruption boreal winter, averaged across eight realizations for each ENSO precondition. The results reveal a distinct cooling pattern over MENA, accompanied by warming over high-latitude Eurasia and the southeastern United States, consistent with previous studies of the Pinatubo eruption. Notably, the strongest cooling occurs under El Niño preconditioning, suggesting that El Niño dynamics amplify the temperature anomalies via enhanced NAO-like features[14]. However, substantial cooling is also observed in the neutral and La Niña scenarios, albeit weaker than in the El Niño case. This challenges previous claims that El Niño is necessary for driving post-eruption NAO-like responses[14], instead suggesting that volcanic forcing alone can initiate such responses, with ENSO playing an amplifying rather than essential role.

To further investigate the underlying mechanisms, we examined surface pressure anomalies (Fig. 2d–f). The results confirm a canonical positive NAO pattern, characterized by high pressure over the Azores and low pressure over Iceland. This pattern supports the notion that volcanic eruptions trigger a positive NAO, which in turn contributes to MENA cooling. The corresponding geopotential height anomalies at 50 hPa (Fig. 2g–i) further reinforce this conclusion, showing strong positive anomalies over mid-latitudes and negative anomalies over the polar region, indicative of a strengthened polar vortex. These results are statistically significant at the 95% confidence level, affirming the robustness of the volcanic-induced NAO response.

To provide a more detailed dynamical perspective, Fig. 3 presents zonally averaged temperature anomalies (left panels) and zonal wind (U-wind) anomalies (right panels) as a function of latitude (0–90°N) and pressure (hPa). These anomalies reflect the difference between volcanic simulations and their respective control runs during the first post-eruption winter under the three ENSO-preconditioned states: El Niño (a, b), neutral (c, d), and La Niña (e, f).

The temperature anomalies (Fig. 3a, c, e) reveal a characteristic dipole structure, with pronounced cooling in the high-latitude stratosphere (60–80°N) and significant warming in the lower stratosphere at lower latitudes (0–60°N). Additionally, an altitudinal temperature gradient emerges, featuring stratospheric warming and tropospheric cooling. These features, particularly evident in the El Niño-preconditioned case (Fig. 3a), are indicative of a strengthened polar vortex, consistent with earlier studies[24,39]. The zonal wind anomalies (Fig. 3b, d, f) further corroborate this interpretation, showing enhanced mid-latitude westerlies (positive U-wind anomalies) at 50–60°N, aligning with the positive NAO response. The strongest westerly anomalies appear under El Niño conditions (Fig. 3b),

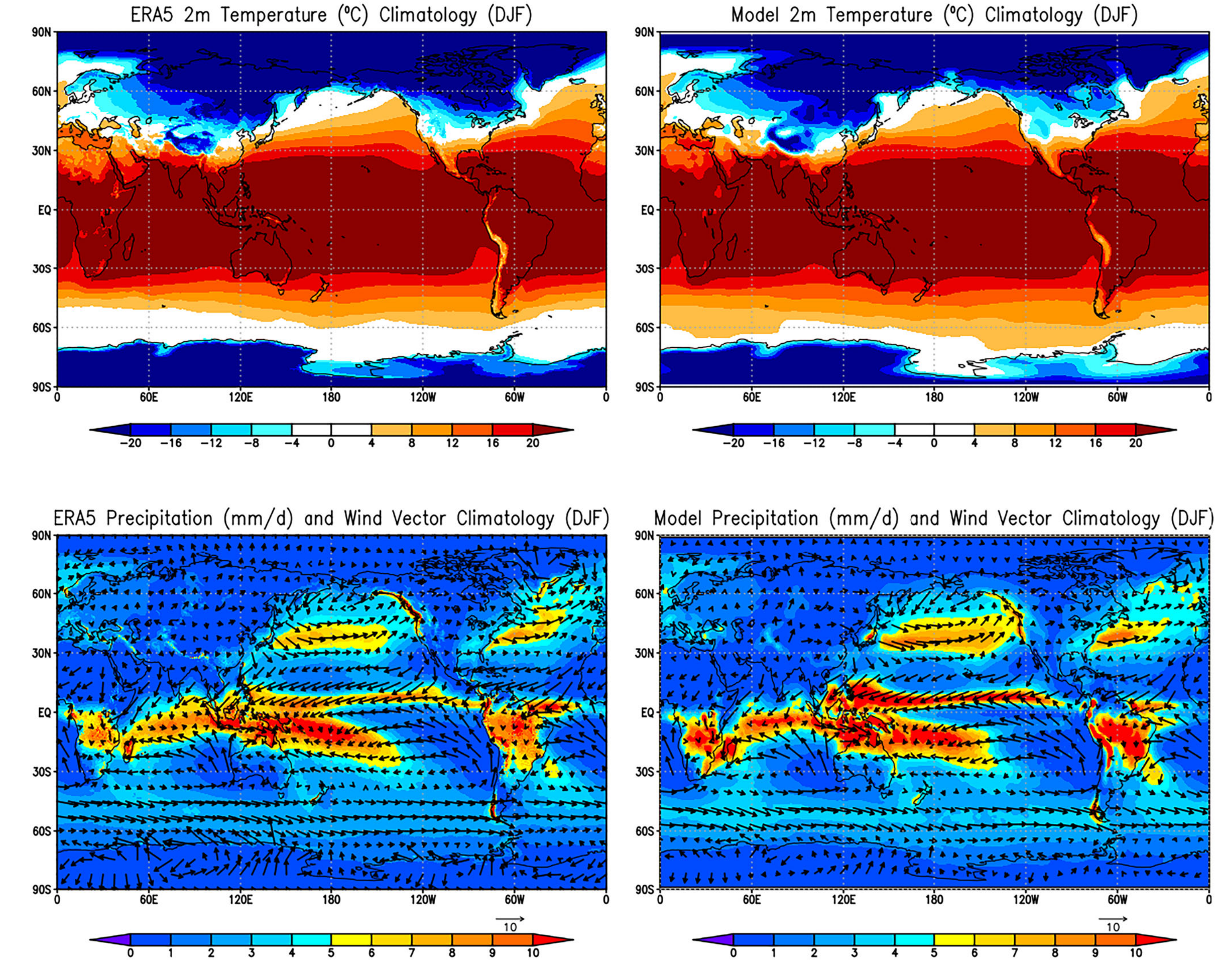

Fig. 1 | Boreal winter climatology from ERA5 and MIROC6. DJF climatological patterns from ERA5 reanalysis (1941–2002; left panels) and the MIROC6 control simulation (model hypothetical years 1941–2002 with forcings fixed at 1991 levels; right panels), showing 2 m surface air temperature (°C, top panels) and precipitation (mm day^{-1}, bottom panels) with overlaid 10 m wind vectors (m s^{-1}).

suggesting that El Niño enhances volcanic impacts on polar vortex dynamics and the NAO[14]. To further clarify the vertical structure of the zonal wind anomalies, we generated an additional plot using logarithmic pressure coordinates (see Supplementary Fig. S6). This vertical scaling allows for a more accurate depiction of the upper troposphere and lower stratosphere, which were visually compressed in the original linear pressure plots. The new figure reveals that under El Niño preconditioning, the zonal-mean westerly anomalies are strongest in the upper troposphere–lower stratosphere region, between ~100 hPa and 10 hPa, indicating a vertically confined and equatorward-enhanced structure. This pattern is consistent with a contracted and poleward-shifted polar vortex, rather than a weakened circulation. These dynamics align well with the observed surface pressure anomalies and the enhanced MENA cooling shown in Fig. 2. The positive NAO phase has distinct regional climate effects, particularly over MENA. The intensified westerlies associated with the volcanic-induced positive NAO phase lead to a northward shift of the Atlantic storm track, enhancing warm air advection and storm activity over Eurasia and northern Europe. Meanwhile, the MENA region lies under the influence of subsiding air and anomalous northerly flow, favoring cold-air advection from higher latitudes and resulting in cooler, drier conditions—consistent with the canonical NAO+ pattern[7,40,41]. The temperature anomalies (Fig. 3a, c, e) reinforce these surface-level effects, directly linking them to volcanic-induced polar vortex strengthening and subsequent tropospheric cooling over MENA (Supplementary Figs. S7 and S8).

These findings highlight the crucial role of volcanic forcing in reshaping atmospheric circulation through a combination of radiative and dynamical processes. The dipole temperature pattern strengthens the equator-to-pole gradient, reinforcing polar vortex intensification and sustaining a positive NAO phase. The corresponding zonal wind anomalies provide additional evidence of this dynamical shift, with mid-latitude westerlies intensifying across all ENSO-preconditioned states, albeit with varying magnitudes.

The zonal-mean diagnostics in Fig. 3 provide compelling evidence that volcanic eruptions, independent of ENSO, can initiate a strengthened polar vortex and a positive NAO response, which in turn drive MENA cooling and Eurasian warming. The MIROC6 model effectively captures these volcanic impacts, particularly under El Niño preconditioning, in agreement with previous findings. However, it is important to note that El Niño-like features observed in prior studies[11] emerge weakly in the first post-eruption winter in MIROC6 but become more pronounced in the second post-eruption winter (not shown). This suggests that while MIROC6 effectively captures the broader effects of volcanic forcing, it does not fully replicate the precise timing of El Niño-like responses, implying timing discrepancies. However, underlying differences in dynamical processes cannot be ruled out.

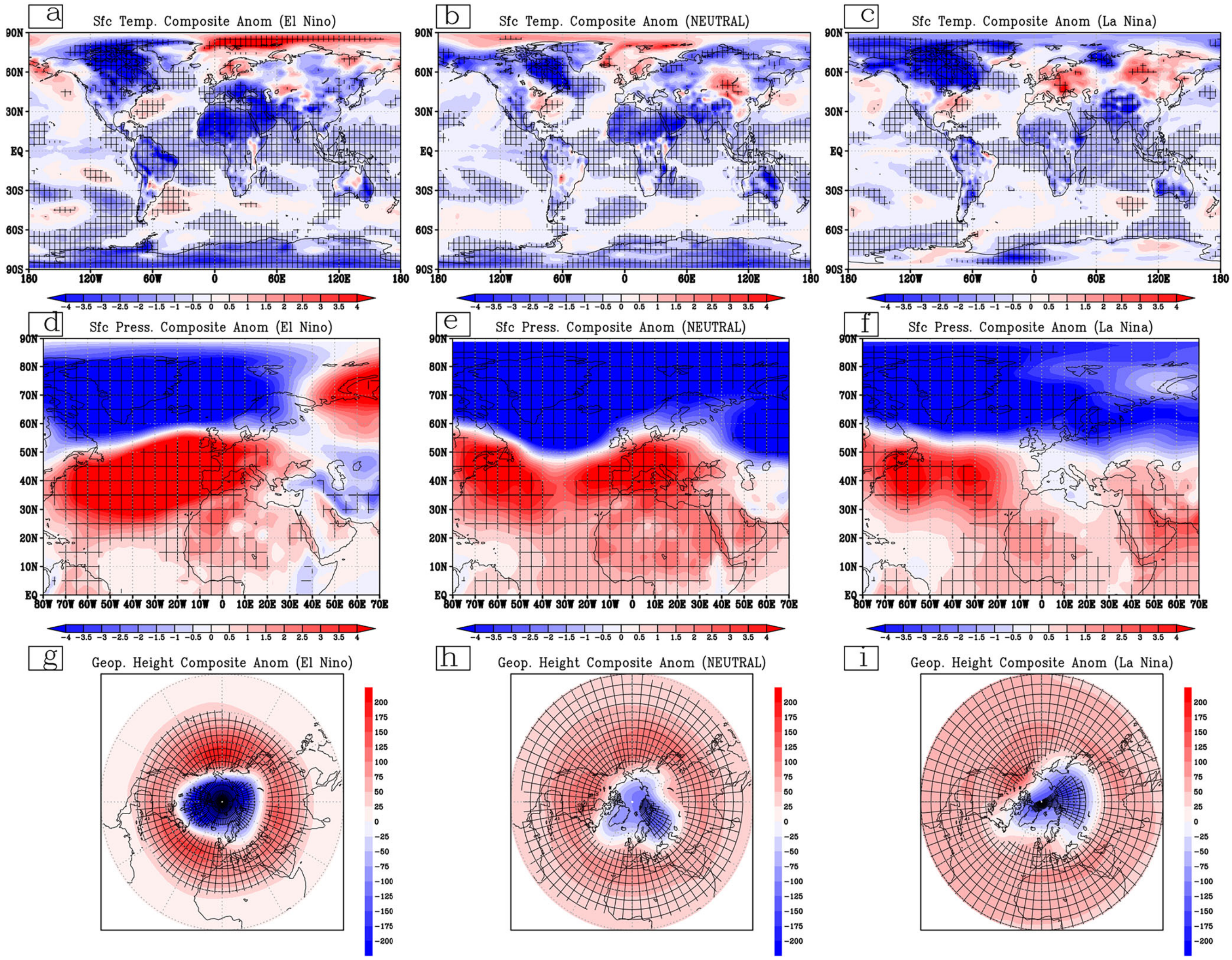

Fig. 2 | Post-eruption boreal winter surface and circulation anomalies under different ENSO states. The top panels illustrate surface (2 m) air temperature anomalies (volcanic simulation minus the coresponding control; °C) for the first post-eruption boreal winter over the entire globe, averaged across eight ensemble members for sensitivity experiments preconditioned with El Niño (**a**), neutral (**b**), and La Niña (**c**) oceanic states. The middle panels (**d**–**f**) show surface pressure anomalies (volcanic simulation minus the corresponding control; hPa) for the same experiments and periods, also averaged over eight ensemble members. Hatched areas indicate statistically significant anomalies at the 95% confidence level, based on a two-sided Student's *t*-test. The bottom panels present geopotential height anomalies at 50 hPa (volcanic simulation minus the coresponding control; m) for the first post-eruption winter, averaged across eight ensemble members for El Niño (**g**), neutral (**h**), and La Niña (**i**) ENSO-preconditioned oceanic states.

Our results indicate that volcanic-induced NAO variability, rather than ENSO, is the primary driver of post-eruption MENA cooling and Eurasian winter warming. While the strongest MENA cooling occurs in El Niño-preconditioned simulations, substantial cooling is also observed under neutral and La Niña conditions, reinforcing the idea that ENSO modulates but does not fundamentally determine the volcanic climate response. This is consistent with earlier findings[14], which suggest that El Niño enhances NAO-like features rather than initiating them. The spatial inconsistencies in high-latitude warming patterns across ENSO states[11] highlight the importance of ocean preconditioning in shaping the magnitude of climate anomalies.

Overall, these findings underscore the dominance of volcanic forcing in driving NAO-like circulation shifts, independent of ENSO, with significant implications for understanding post-eruption climate variability in MENA and beyond.

Post-volcanic MENA summer response—influence of ENSO dynamics

Previous studies have suggested that post-eruption circulation changes, both direct and indirect, lead to significant mid-latitude cooling in MENA and tropical warming over the Intertropical Convergence Zone (ITCZ) and tropical convective regions. These effects have primarily been examined using atmospheric global or regional models[7,8], which have limited vertical resolution, hindering their ability to fully capture stratospheric processes. In this study, we use the high vertical-resolution, high-top MIROC6 coupled global climate model to more effectively analyze these cooling and warming features.

Figure 4 illustrates the summer response during the first summer following the eruption. It is important to note that we did not display the summer during which the eruption occurred—such as the Pinatubo eruption occurred in June 1991—and we display the subsequent summer period, that is summer (JJA) 1992 as this will be having stronger impacts of volcanism rather than the concurrent summer period (i.e., JJA 1991) during which eruption occurred. Our results reveal a pronounced cooling response in mid-latitude regions across all ENSO-preconditioned states. Additionally, tropical warming (reaching to 1 °C) is observed over the convective regions of the ITCZ, especially for El Nino-preconditioned case (see Fig. 4a), which is consistent with previous findings[7,42].

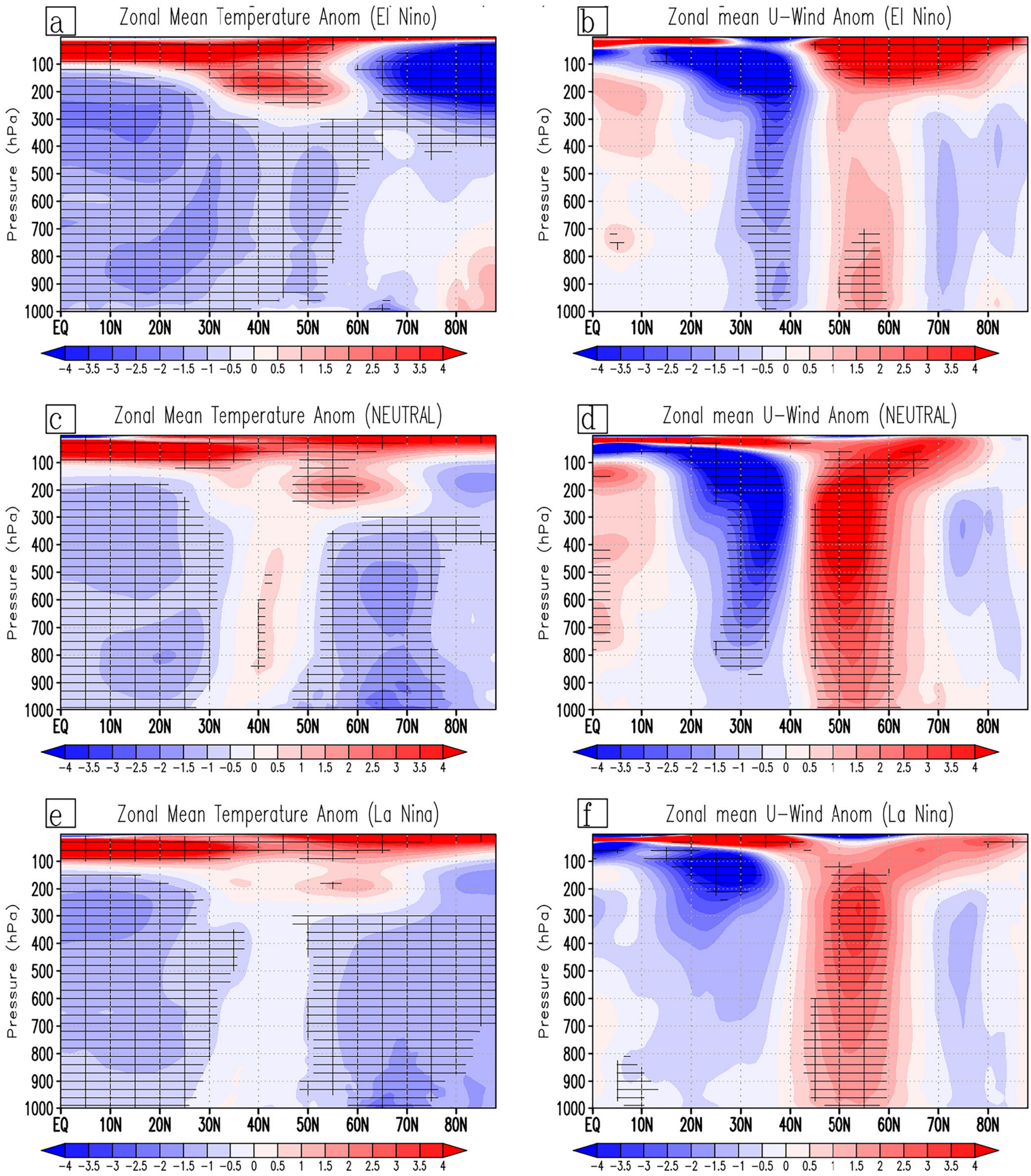

Fig. 3 | Post-eruption zonally averaged temperature and zonal wind (U-wind) anomalies. Left panels show zonally averaged air temperature anomalies (volcanic simulation minus control; °C) as a function of latitude (*x*-axis, 0–90°N) and pressure (*y*-axis, hPa) during the first post-eruption boreal winter (DJF 1991/1992), averaged across eight ensemble members for sensitivity experiments preconditioned with El Niño (**a**), Neutral (**c**), and La Niña (**e**) oceanic states. Right panels (**b**, **d**, **f**) depict zonally averaged zonal wind anomalies (volcanic simulation minus control; m/s) for the same experiments and period, also averaged across eight ensemble members. Hatched areas denote statistically significant anomalies at the 95% confidence level, determined using a two-sided Student's *t*-test. Note: The zonal-mean representation is intended to illustrate large-scale stratosphere–troposphere dynamical responses (e.g., polar vortex modulation and NAO phase), which influence surface climate over multiple regions including the Middle East and North Africa (MENA), broadly defined here as spanning 5°S to 45°N latitude and 20°W to 70°E longitude.

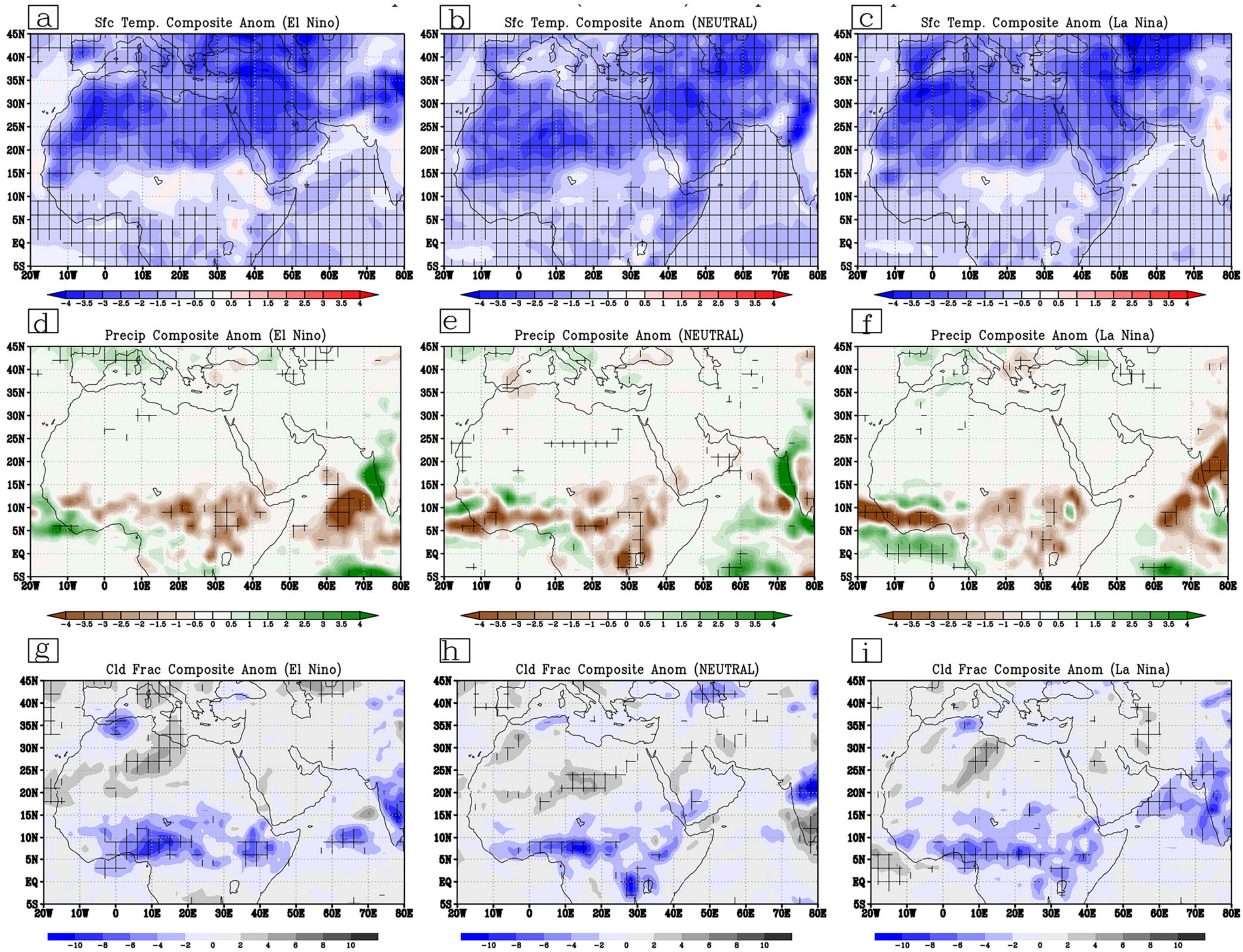

Fig. 4 | Post-eruption surface temperature, precipitation, and cloud fraction anomalies over MENA. The top panels illustrate surface (2 m) air temperature anomalies (volcanic simulation minus the corresponding control; °C) for the post-eruption summer (JJA 1992) over the MENA region (5°S–45°N, 20°W–70°E), averaged across eight ensemble members for sensitivity experiments preconditioned with El Niño (**a**), neutral (**b**), and La Niña (**c**) oceanic states. The middle panels (**d**–**f**) show surface precipitation anomalies (volcanic simulation minus the corresponding control; mm/d) for the same experiments and periods, also averaged over eight ensemble members. Hatched areas indicate statistically significant anomalies at the 95% confidence level, based on a two-sided Student's *t*-test. The bottom panels show cloud fraction anomalies (volcanic simulation minus the corresponding control; %) at 550 level for post-eruption summer period (i.e., JJA 1992), averaged across eight ensemble members for El Niño (**g**), neutral (**h**), and La Niña (**i**) ENSO-preconditioned oceanic states.

Notably, the cooling and warming anomalies are more pronounced in the El Niño-preconditioned case, suggesting that the El Niño preconditions during the Pinatubo eruption could further amplify these effects. Figure 4d–f shows the precipitation response, with a marked decrease in precipitation over the ITCZ region in all three ENSO-initialized cases. However, a noticeable shift in the ITCZ is observed, particularly in the El Niño-initialized case. This southward shift in the ITCZ suggests that the El Niño-like pattern enhances the weakening of the ITCZ, which aligns with earlier studies (Dogar et al.[7]; Haywood et al.[32]) that used HiRAM AGCM to investigate post-eruption summer responses in MENA. Additionally, over Southern Europe, our simulated precipitation anomalies show good agreement with findings from Wegmann et al.[43], who reported similar volcanic-induced wetting and drying patterns in the Northern Mediterranean. This agreement further supports the robustness of our ENSO-preconditioned ensemble approach in capturing regionally nuanced hydrological responses to tropical volcanic forcing.

This shift in ITCZ can be attributed to the latitudinal thermal gradient induced by the tropical eruption, which suppresses the intrusion of moisture from the Indian and Atlantic Oceans into the MENA inland regions. This suppression is further corroborated by the decreased cloud cover in the ITCZ region (Fig. 4g–i), which shows a reduction in cloud cover following the eruption. The diminished cloud cover facilitates increased downwelling solar radiation, warming the tropical ITCZ convective zone, as reflected in the temperature anomaly patterns.

Based on the results depicted in Fig. 4, we conclude that the post-eruption summer cooling in mid-latitude MENA, along with the warming and decreased precipitation due to the weakened ITCZ (i.e., the upward branch of the Hadley Cell), are primarily driven by the combined impacts of direct and indirect circulation changes. These changes are mediated by ENSO and the Indian Ocean Dipole or by impacts on the Indian Monsoon, consistent with prior studies[7,42].

While this section discusses tropical features such as the ITCZ and associated convection patterns, the purpose is to provide a physical explanation for the observed post-volcanic summer anomalies over the MENA region. The drying and cooling signals over MENA are dynamically linked to changes in tropical circulation and moisture transport. Therefore, the analysis of tropical responses serves to contextualize and mechanistically interpret the regional climate impacts in MENA during the post-eruption summer.

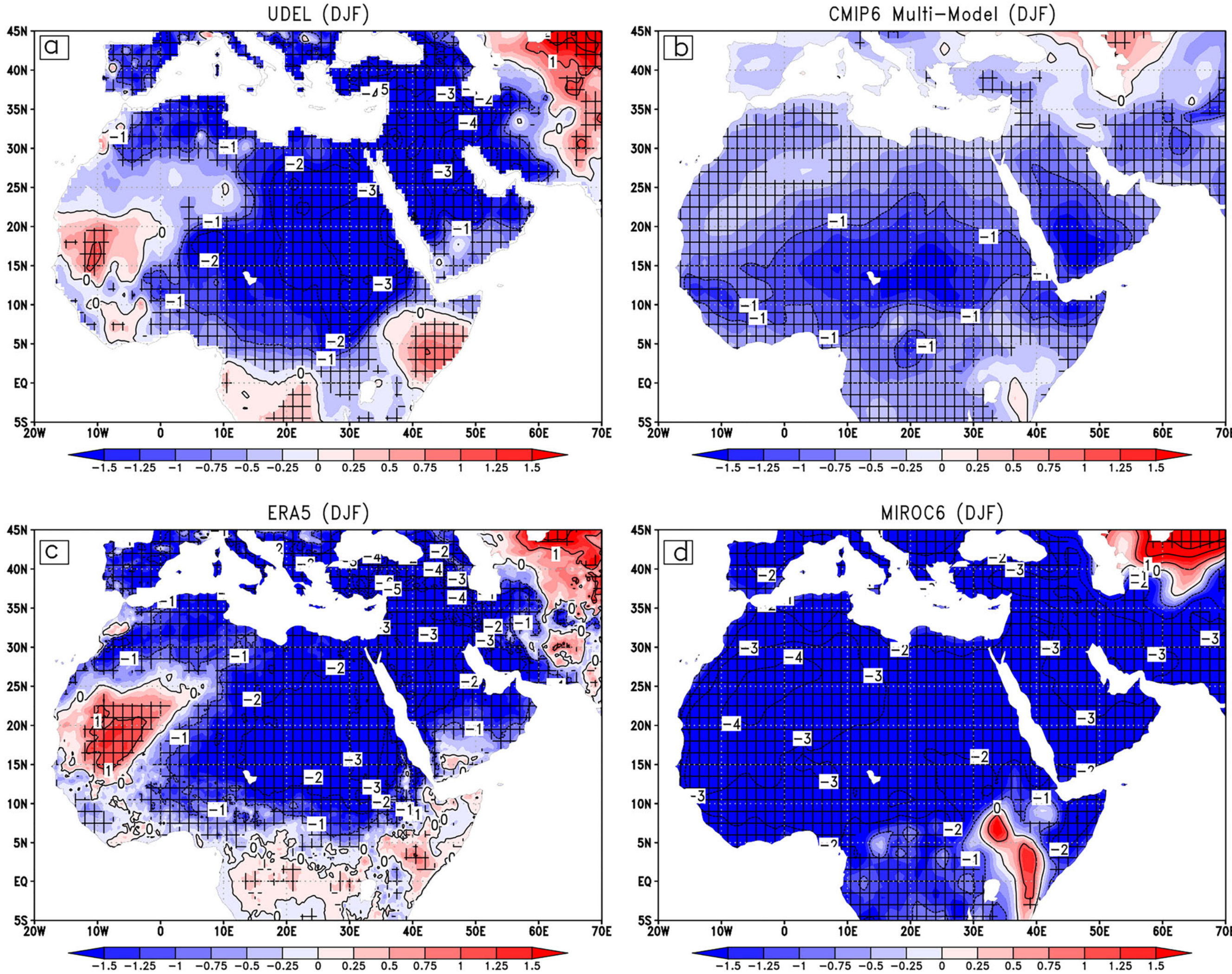

Fig. 5 | Near-surface air temperature anomalies during the first post-eruption winter. Spatial distribution of near-surface air temperature anomalies (°C) during DJF 1991/1992 (first post-eruption winter) from **a** UDEL observations, **b** CMIP6 historical multi-model ensemble mean, **c** ERA5 reanalysis, and **d** our idealized MIROC6 ensemble simulation (El Niño-initialized, 3× Pinatubo forcing). Hatched areas indicate statistical significance at the 95% confidence level based on a two-tailed Student's *t*-test. Anomalies for (**a**–**c**) are calculated relative to the 1991–2002 DJF climatology (excluding 1991/1992 and 1992/1993), and for (**d**) relative to the corresponding MIROC6 control run without volcanic forcing.

Comparison with observations, reanalysis, and CMIP6 models

To further evaluate the robustness and physical consistency of our model results, we compare the surface temperature anomalies during the first post-eruption winter (DJF 1991/1992) and summer (JJA 1992) using four independent data sources: (i) UDEL gridded observations (Willmott and Matsuura[44]), (ii) ERA5 reanalysis, (iii) CMIP6 historical multi-model ensemble mean based on six models (UKESM1-0-LL, CESM2 WACCM, CESM2, MIROC6, MRI-ESM2-0, and GFDL-ESM4), each with a single ensemble member (r1i1p1f1) obtained from the Copernicus Climate Data Store (CDS), and (iv) our idealized MIROC6 ensemble simulations (El Niño-initialized case with 3× Pinatubo forcing).

For consistency, anomalies in UDEL, ERA5, and the CMIP6 ensemble are calculated relative to a 1991–2002 seasonal climatology (excluding 1991/1992 and 1992/1993 for DJF, and 1991 and 1992 for JJA), while anomalies in our MIROC6 simulations are calculated relative to a non-volcanic control simulation. Both the control and volcanic simulations use fixed boundary conditions (e.g., greenhouse gas concentrations, solar irradiance, land use, and tropospheric ozone held constant at 1990 levels). Stratospheric ozone responds to volcanic forcing via prescribed ozone fields in the volcanic simulation.

Despite differences in experimental setups, such as real-world versus idealized forcing magnitudes and evolving versus fixed boundary conditions, the large-scale patterns are broadly consistent across datasets.

In DJF (Fig. 5), all four sources exhibit significant surface cooling over the MENA region, particularly over the Arabian Peninsula and the eastern Mediterranean. Minor regional warming patches seen in UDEL and ERA5 are likely due to residual internal variability. The multi-model CMIP6 mean smooths out much of this noise, while our MIROC6 ensemble, with its amplified 3× Pinatubo forcing, shows stronger but spatially coherent signals.

In JJA (Fig. 6), all datasets reveal cooling over the northern parts of MENA, along with a notable warming anomaly over the low-latitude MENA tropical belt, particularly between 10°N and 20°N, i.e., south of ~20°N. This feature is a well-known post-eruption dynamical signal associated with the southward displacement of the ITCZ, resulting in clearer skies, reduced rainfall, and increased solar radiation (Dogar et al.[7]). This pattern is well captured in the CMIP6 ensemble and our MIROC6 simulations, reinforcing its dynamical robustness and relevance to volcanic forcing over the region.

Interestingly, UDEL and ERA5 show stronger anomalies than the CMIP6 ensemble mean, in agreement with prior studies suggesting that

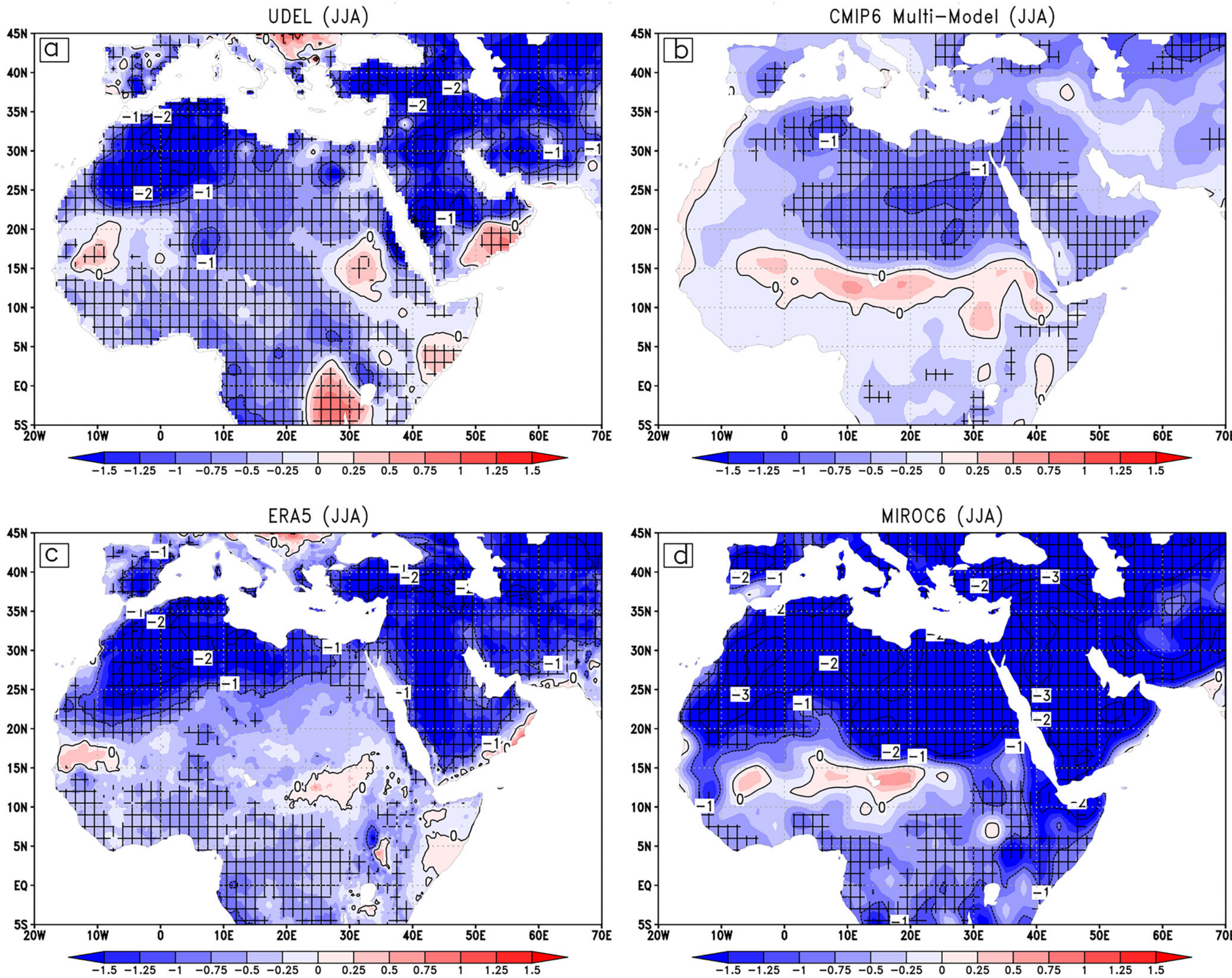

Fig. 6 | Same as Fig. 5, but for JJA 1992 (i.e., second post-eruption summer). Anomalies for (**a**–**c**) are relative to the 1991–2002 JJA climatology (excluding 1991 and 1992), and for (d) relative to the corresponding MIROC6 control run without volcanic forcing.

models tend to underestimate the magnitude of circulation-driven responses, such as those related to ENSO and NAO, following volcanic eruptions (Dogar et al.[7]). Our idealized simulations exhibit stronger responses due to the enhanced forcing, but maintain realistic spatial structures consistent with empirical data.

Together, these results confirm that the post-eruption temperature responses simulated by our idealized MIROC6 model are not artifacts of a single-model framework, but rather reflect robust, physically meaningful signals that are consistent with real-world observations and state-of-the-art reanalysis and modeling systems. This strengthens the confidence in the model's sensitivity and the relevance of its findings for understanding regional climate responses to volcanic forcing.

Discussion

The simultaneous occurrence of strong volcanic eruptions and large-scale circulation changes driven by natural variability, such as ENSO and NAO, complicates efforts to isolate volcanic effects from underlying climate patterns. Historical observations indicate significant winter warming in high-latitude Eurasia and amplified winter cooling in the MENA following tropical volcanism. These changes have been linked to polar vortex strengthening and a positive NAO phase[22,39,45–49]. Similarly, post-eruption summer cooling in high-latitude regions of MENA, along with tropical warming and changes in precipitation patterns, are attributed to both direct and indirect circulation shifts[7,42]. Despite these observed associations, climate models still struggle to replicate the post-eruption dynamics of NAO and ENSO, particularly across different seasons in the MENA region.

The coexistence of robust volcanic forcing and natural ENSO variability raises important questions about the primary drivers of winter warming in Eurasia and cooling in MENA. This suggests that ENSO teleconnections, rather than volcanic impacts alone, may be responsible[3,5,15]. Recent studies propose a synergistic role for volcanic activity and El Niño conditions in triggering positive NAO phases, leading to warm winters over Eurasia and cold winters across MENA and South Asia[7,14]. These findings, combined with complex volcano-ENSO and volcano-NAO interactions, highlight the difficulty in identifying the precise source of post-volcanic winter cooling and summer warming, along with associated drying in the tropical MENA region.

A significant divide persists among climate models, observational data, and proxy reconstructions in understanding the relationships between volcanic activity, ENSO, and NAO, particularly regarding their post-volcanic impacts. These impacts include warming in high-latitude regions and cooling in lower-latitude areas[3,5,7,14,15,48,50]. To address these discrepancies, we conducted numerical sensitivity experiments using the MIROC6 coupled atmosphere-ocean model to explore how ENSO preconditioning influences post-volcanic ENSO evolution and how volcanic-induced ENSO and NAO variability affect the MENA region, particularly in terms of amplified winter cooling and summer tropical warming and drying.

While our idealized ensemble experiments using MIROC6 provide robust insights into stratosphere–troposphere coupling and ENSO–NAO interactions under strong volcanic forcing, we acknowledge that the empirical basis could be further strengthened through multi-model intercomparisons, paleoclimate reconstructions, and extended reanalysis-based validation. Future studies incorporating these approaches will be essential to test the robustness and generalizability of our findings across different model configurations and observational records.

In future work, it would be valuable to design controlled experiments with symmetric and well-defined ENSO phase characteristics (e.g., type, strength, and spatial structure) to systematically assess the differential modulation of post-volcanic responses across ENSO states through direct anomaly comparisons.

While we hypothesized that strong volcanic forcing could trigger nonlinear or threshold-like responses in the tropical climate system, our present results did not reveal any distinct tipping behavior. A more comprehensive assessment would require a broader ensemble and multiple forcing levels to systematically explore response nonlinearity. This remains an important direction for future research.

Although our analysis focused primarily on stratospheric responses and mid-latitude teleconnections (e.g., NAO and polar vortex dynamics), we acknowledge that the subtropical jet and its interaction with the Asian monsoon system may play an important upstream role in shaping volcanic–ENSO teleconnections. These features influence the propagation of planetary waves and the modulation of stratosphere–troposphere coupling. A more detailed investigation of these interactions, including their influence on MENA climate via monsoon–jet dynamics, represents an important direction for future research.

Our perturbation experiments reveal that the ENSO response to volcanic eruptions is strongly influenced by the pre-existing ocean state. Specifically, El Niño preconditioning results in a more pronounced anomalous response, while neutral or La Niña conditions produce weaker responses. Contrary to prior expectations, our model experiments suggest that post-eruption MENA winter cooling is primarily driven by volcanic-induced NAO patterns rather than ENSO variability. Moreover, the presence of an El Niño-like preconditioning pattern is not necessary for significant winter cooling; powerful volcanic eruptions alone are sufficient to induce pronounced cooling in MENA through both direct and indirect mechanisms. These findings highlight the critical role of the NAO in modulating post-volcanic climate dynamics in MENA, with ENSO preconditioning acting as an amplifying factor rather than the primary driver. Our MIROC6-based idealized experiments strongly support the conclusion that post-eruption amplified cooling in MENA is largely a result of NAO variability driven by volcanic activity, with ENSO preconditions enhancing this cooling during the winter months.

In the summer following volcanic eruptions, stronger tropical eruptions produce cooling in high-latitude MENA regions, while warming and drying are observed in the tropical convective zone. This pattern results from a weakened thermal gradient between the ocean and inland MENA regions, which suppresses the upward branch of the Hadley Cell and reduces moisture availability. This behavior is consistent with previous studies and further affirms the effectiveness of the high-top MIROC6 model in capturing both the direct and indirect impacts of volcanic activity.

Our study highlights the utility of the moderate-resolution, coupled global climate model (MIROC6) in capturing the link between volcanic eruptions and NAO through stratosphere–troposphere interactions. This finding suggests the need for models with higher atmospheric vertical resolution to better represent these interactions and their impacts. The MIROC6 model's ability to reproduce the strengthening of the polar vortex, positive NAO-like patterns, high-latitude warming, and MENA cooling underscores its efficacy in simulating post-volcanic climate responses. Furthermore, the model's representation of mid-latitude MENA winter cooling, summer tropical warming, and reduced precipitation due to cloud cover changes further affirms its capability to simulate the complex regional impacts of volcanic eruptions.

In conclusion, this study advances our understanding of post-eruption climate impacts, particularly the specific role of volcanic-induced NAO variability in driving amplified cooling in MENA. Insights derived from the MIROC6 model make significant contributions to volcanic impact research and provide valuable guidance for policy studies related to eruption-driven climate fluctuations.

While our study specifically focuses on a single tropical eruption scenario (based on the Pinatubo case) during boreal summer with enhanced stratospheric aerosol loading, we acknowledge that other important dimensions—such as the eruption season, latitude, and the vertical profile of aerosol injection—can significantly modulate the climate response. These factors influence stratospheric circulation, radiative forcing, and the resulting teleconnections. Future studies using a broader ensemble of eruption scenarios and more realistic aerosol vertical distributions will be essential to explore the full parameter space of volcanic impacts.

Although this study focuses on ENSO–NAO interactions in modulating post-volcanic climate responses, it is worth noting that the stratospheric quasi-biennial oscillation (QBO) may also play a role in shaping the dynamical response to tropical eruptions. The phase of the QBO can influence stratospheric wave propagation and polar vortex strength, potentially altering the extratropical response to volcanic aerosols[45,51,52]. While our ensemble design does not explicitly resolve or control for QBO variability, we acknowledge its potential relevance and recommend that future studies incorporate QBO phase-resolving experiments to more comprehensively assess its modulation of post-eruption climate impacts.

Finally, our results are further supported by comparisons with observational, reanalysis, and CMIP6 ensemble data, which reveal broadly consistent temperature anomaly patterns during both the first post-eruption winter (DJF 1991–92) and the second post-eruption summer (JJA 1992). The focus on JJA 1992 is intentional, as the climatic response to the Pinatubo eruption, which occurred in June 1991, typically matures over time and becomes more pronounced by the second summer. This consistency reinforces the credibility of our modeled results and confirms the physical robustness of the volcanic signal, particularly over the MENA region.

Methods

This study utilizes the MIROC6 coupled model to investigate the post-volcanic climatic impacts on winter and summer seasons in the MENA region (for details, see section "Model description and numerical model experiments"). To assess the influence of ENSO (El Niño, La Niña, and Neutral) on volcanic climate variability in the MENA region, we analyze key climate indices: the ENSO (Niño3.4) and NAO indices. The Niño3.4 index represents the average sea surface temperature anomalies over the NINO3.4 region (5°N–5°S; 170°W–120°W), providing a standardized measure of ENSO states. The NAO index is derived from the normalized sea-level pressure (SLP) difference between the Lisbon region in Portugal (~38.7°N, 9.1°W) and the Stykkisholmur/Reykjavik region in Iceland (~65.1°N, 21.9°W), following the method of Hurrell[41], which captures key modes of atmospheric pressure variability over the North Atlantic.

For statistical analysis, we apply the Student's two-tailed t-test to assess the significance of composited post-volcanic winter and summer anomalies, with significance evaluated at the 95% confidence level, considering the appropriate degrees of freedom ($N-2$, where N is the number of years). This approach follows established practices in climate research, consistent with previous studies[7,11].

Model description and numerical model experiments

To examine the sensitivity of ENSO and NAO to large tropical volcanic events and their climatic effects in the MENA region, we employ the sixth version of the Model for Interdisciplinary Research on Climate (MIROC6), a state-of-the-art coupled atmosphere-ocean global circulation model developed by the Japanese modeling community. MIROC6 is an improved version of its predecessor, MIROC5, and has demonstrated strong performance in detecting atmospheric and oceanic teleconnections[53]. This model is widely used in CMIP6-based impact studies but exhibits a relatively weaker atmospheric response for NAO-type variability, a limitation shared by many coupled models[10,33]. Comprehensive details of MIROC6's formulation and simulation characteristics are provided in ref. 53.

MIROC6 operates at a horizontal resolution of ~150 km (i.e., T85, 1.4°) and is classified as a "high-top" model, extending up to ~0.004 hPa (81 vertical levels). Unlike low-top models in CMIP3 and CMIP5, which struggle to accurately simulate the post-eruption intensification of the polar vortex and related NAO dynamics[7,10,52], MIROC6 has shown better performance in simulating the impacts of natural variability[53,54]. The MIROC6 used in the present study includes further improvements beyond the CMIP6 version: (1) the number of vertical levels in the lower stratosphere was increased to 90 to enhance the amplitude of the equatorial QBO and improve vertical dynamical coupling between the stratosphere and troposphere, particularly in relation to polar vortex variations; (2) the surface topography was modified from a grid-mean elevation to a silhouette-based orographic representation, snow surface roughness was reduced, and the turbulence orography form drag scheme of Beljaars[54,55] was introduced to improve low-level wind and temperature biases.

Despite its improvements, the model's response to volcanic eruptions remains relatively unexplored. This study serves as a pioneering investigation into MIROC6's sensitivity to volcanic events and their interaction with natural climate variability, such as ENSO and NAO.

To explore regional climate responses in the MENA region, we focus on the Mount Pinatubo eruption of June 1991, amplifying its aerosol loading to three times the observed levels[56]. This enhanced scenario reflects previous research suggesting that stronger eruptions may better capture ENSO's response to volcanic forcing[11,57]. By simulating aerosol loading at three times the Pinatubo strength, we aim to explore potential nonlinear climate responses, such as amplified teleconnections or threshold-like sensitivities, while also enhancing signal detectability. Although this study does not explicitly quantify nonlinearities, the experimental framework is designed to enable such investigations in future ensemble-based or multi-magnitude studies.

To amplify the forced signal and reduce the influence of internal variability, we applied a stratospheric aerosol optical depth equivalent to three times the magnitude of the 1991 Mount Pinatubo eruption. This idealized approach is commonly used in volcanic climate studies to improve the signal-to-noise ratio and isolate dynamical mechanisms in regions where volcanic impacts are subtle or seasonally masked[9,14,58]. In addition to enhancing signal detectability, this forcing strength allows for the exploration of nonlinear and potentially threshold-dependent responses in the coupled climate system, particularly in terms of stratosphere–troposphere coupling and ENSO–NAO teleconnections. While eruptions of this magnitude are rare in the modern instrumental record, they remain plausible based on paleoclimate reconstructions (e.g., Samalas in 1257, Tambora in 1815). A full sensitivity analysis of eruption magnitude is beyond the scope of this study but remains an important direction for future research.

The enhanced volcanic forcing was incorporated into the MIROC6 model using spectral-dependent aerosol characteristics, consistent with historical volcanic eruptions. The volcanic-related radiative fluxes were calculated using the Discrete Ordinate Method and the k-distribution Method[59], with updates from Sekiguchi and Nakajima[60], to model absorption, emission, and scattering processes by gases and aerosols.

Three volcanic experiments were conducted, each initialized with distinct ENSO conditions: El Niño, Neutral, and La Niña. These initial ENSO states were selected from a 100-year MIROC6 long control run (Supplementary Fig. S1), ensuring persistence of each state for at least 1.5 years. For both the volcanic and control simulations, all forcing factors—including solar irradiance, aerosols, greenhouse gases, ozone, and other forcings—were fixed at 1990 levels to closely align with the eruption timing of Pinatubo. The Niño3.4 indices used to define ENSO conditions were greater than +0.5 °C for El Niño, less than −0.5 °C for La Niña, and between −0.5 °C and +0.5 °C for Neutral. Each selected ENSO initialization (El Niño, Neutral, and La Niña) starts from January month, aligning with the seasonal dynamics of ENSO and ensuring robust initial conditions. The enhanced volcanic forcing (three times the Pinatubo strength) was applied in June 1991, coinciding with the actual eruption month. Each ENSO-initialized scenario included a corresponding control run with identical initial conditions but without volcanic forcing. This approach allowed us to isolate the climatic impacts of volcanic aerosols under varying ENSO states.

Each ENSO-preconditioned volcanic experiment comprised eight ensemble members, initialized with slightly perturbed initial conditions, following methodologies established by Dogar et al.[11,61]. Simulations were performed for a 12-year period (1991–2002) for each scenario, and results were presented as composite averages across the ensemble members.

To isolate volcanic impacts and reduce potential climate drift, results are presented as anomalies by subtracting control (no-volcano) runs from the volcanic simulations[61]. This differential approach aligns with methodologies used in prior studies[11,20,61]. The reported model years are symbolic/hypothetical, reflecting the experimental design rather than historical timelines.

Data availability

This study utilized multiple publicly available datasets. The ERA5 reanalysis dataset is accessible via the European Centre for Medium-Range Weather Forecasts (ECMWF) at https://www.ecmwf.int/en/forecasts/datasets/browse-reanalysis-datasets. The University of Delaware (UDEL) gridded temperature dataset can be obtained from https://psl.noaa.gov/data/gridded/data.UDel_AirT_Precip.html. Historical simulations from various CMIP6 models were retrieved from the Copernicus Climate Data Store (CDS) at https://cds.climate.copernicus.eu/datasets/projections-cmip6. Ensemble simulations produced using the MIROC6 AOGCM are available from the corresponding author upon reasonable request.

Code availability

The figures in this study were all plotted using the Grid Analysis and Display System (GrADS), as detailed in http://cola.gmu.edu/grads/. All codes are also available from the corresponding author upon reasonable request.

Received: 1 April 2025; Accepted: 12 August 2025;
Published online: 29 September 2025

References

1. Robock, A. Volcanic eruptions and climate. *Rev. Geophys.* **38**, 191–219 (2000).
2. Timmreck, C. Modeling the climatic effects of large explosive volcanic eruptions. *Wiley Interdiscip. Rev. Clim. Change* **3**, 545–564 (2012).
3. Dogar, M. M. et al. A review of El Niño Southern Oscillation linkage to strong volcanic eruptions and post-volcanic winter warming. *Earth Syst. Environ.* **7**, 15–42 (2023).
4. McCormick, M. P., Thomason, L. W. & Trepte, C. R. Atmospheric effects of the Mt Pinatubo eruption. *Nature* **373**, 399–404 (1995).
5. Polvani, L. M., Banerjee, A. & Schmidt, A. Northern Hemisphere continental winter warming following the 1991 Mt. Pinatubo eruption: reconciling models and observations. *Atmos. Chem. Phys.* **19**, 6351–6366 (2019).
6. Tejedor, E., Polvani, L. M., Steiger, N. J., Vuille, M. & Smerdon, J. E. No evidence of winter warming in Eurasia following large, low-latitude volcanic eruptions during the Last Millennium. *J. Clim.* **37**, 5653–5673 (2024).
7. Dogar, M. M., Stenchikov, G., Osipov, S., Wyman, B. & Zhao, M. Sensitivity of the regional climate in the Middle East and North Africa to volcanic perturbations. *J. Geophys. Res. Atmos.* **122**, 7922–7948 (2017).
8. Joseph, R. & Zeng, N. Seasonally modulated tropical drought induced by volcanic aerosol. *J. Clim.* **24**, 2045–2060 (2011).
9. Zambri, B. & Robock, A. Winter warming and summer monsoon reduction after volcanic eruptions in Coupled Model Intercomparison Project 5 (CMIP5) simulations. *Geophys. Res. Lett.* **43**, 10–920 (2016).

10. Swingedouw, D. et al. Impact of explosive volcanic eruptions on the main climate variability modes. *Glob. Planet. Change* **150**, 24–45 (2017).
11. Dogar, M. M., Fujiwara, M., Zhao, M., Ohba, M. & Kosaka, Y. ENSO and NAO linkage to strong volcanism and associated post-volcanic high-latitude winter warming. *Geophys. Res. Lett.* **51**, e2023GL106114 (2024).
12. Genin, A., Lazar, B. & Brenner, S. Vertical mixing and coral death in the Red Sea following the eruption of Mount Pinatubo. *Nature* **377**, 507–510 (1995).
13. Muhammad, M., Dogar, M., Fujiwara, M. & Ohba, M.A. Investigating post-eruption amplified winter cooling in the Middle East and North Africa-unraveling ENSO and NAO dynamics. *Environ. Res. Commun*. **7**, 045012 (2025).
14. Coupe, J. & Robock, A. The influence of stratospheric soot and sulfate aerosols on the Northern Hemisphere wintertime atmospheric circulation. *J. Geophys. Res. Atmos.* **126**, e2020JD034513 (2021).
15. Polvani, L. M. & Camargo, S. J. Scant evidence for a volcanically forced winter warming over Eurasia following the Krakatau eruption of August 1883. *Atmos. Chem. Phys.* **20**, 13687–13700 (2020).
16. Qin, Z., Wang, T., Gao, Y. & Fu, Y. MPI-ESM grand ensemble-simulated influence of the Mount Pinatubo volcanic eruption on winter climate over the mid-to high-latitude Northern Hemisphere continents. *Int. J. Climatol.* **45**, e8719 (2025).
17. Wodon, Q., Liverani, A., Joseph, G. & Bougnoux, N. (eds) *Climate Change and Migration: Evidence from the Middle East and North Africa* (World Bank Publications, 2014).
18. Trenberth, K. E. & Dai, A. Effects of Mount Pinatubo volcanic eruption on the hydrological cycle as an analog of geoengineering. *Geophys. Res. Lett.* **34**, L15702 (2007).
19. Dogar, M. M. Impact of tropical volcanic eruptions on Hadley circulation using a high-resolution AGCM. *Curr. Sci.* **114**, 1284–1294 (2018).
20. Dogar, M. M. A. (2020). Study of the regional climatic impacts of tropical explosive volcanism in the Middle East and North Africa region (Doctoral dissertation, Hokkaido University).
21. McConnell, J. R. et al. Extreme climate after massive eruption of Alaska's Okmok volcano in 43 BCE and effects on the late Roman Republic and Ptolemaic Kingdom. *Proc. Natl. Acad. Sci. USA* **117**, 15443–15449 (2020).
22. Kodera, K. Influence of volcanic eruptions on the troposphere through stratospheric dynamical processes in the northern hemisphere winter. *J. Geophys. Res. Atmos.* **99**, 1273–1282 (1994).
23. Banerjee, A. et al. Robust winter warming over Eurasia under stratospheric sulfate geoengineering—the role of stratospheric dynamics. *Atmos. Chem. Phys.* **21**, 6985–6997 (2021).
24. Stenchikov, G. et al. Arctic Oscillation response to volcanic eruptions in the IPCC AR4 climate models. *J. Geophys. Res.* **111**, D7 (2006).
25. Kim, H., Min, S.-K., Kim, D. & Visioni, D. Volcanically forced Madden–Julian oscillation triggers the immediate onset of El Niño. *Nat. Commun.* **16**, 1399 (2025).
26. Khodri, M. et al. Tropical explosive volcanic eruptions can trigger El Niño by cooling tropical Africa. *Nat. Commun.* **8**, 778 (2017).
27. Liu, F. et al. Tropical volcanism enhanced the East Asian summer monsoon during the last millennium. *Nat. Commun.* **13**, 3429 (2022).
28. Smith, D. M. et al. Role of volcanic and anthropogenic aerosols in the recent global surface warming slowdown. *Nat. Clim. Change* **6**, 936–940 (2016).
29. Bethke, I. et al. Potential volcanic impacts on future climate variability. *Nat. Clim. Change* **7**, 799–805 (2017).
30. Otterå, O. H., Bentsen, M., Drange, H. & Suo, L. External forcing as a metronome for Atlantic multidecadal variability. *Nat. Geosci.* **3**, 688–694 (2010).
31. Booth, B. B., Dunstone, N. J., Halloran, P. R., Andrews, T. & Bellouin, N. Aerosols implicated as a prime driver of twentieth-century North Atlantic climate variability. *Nature* **484**, 228–232 (2012).
32. Haywood, J. M., Jones, A., Bellouin, N. & Stephenson, D. Asymmetric forcing from stratospheric aerosols impacts Sahelian rainfall. *Nat. Clim. Change* **3**, 660–665 (2013).
33. Driscoll, S., Bozzo, A., Gray, L. J., Robock, A. & Stenchikov, G. Coupled Model Intercomparison Project 5 (CMIP5) simulations of climate following volcanic eruptions. *J. Geophys. Res. Atmos.* **117**, D17105 (2012).
34. Luo, F. et al. ENSO-driven abrupt phase shift in North Atlantic Oscillation in early January. *npj Clim. Atmos. Sci.* **6**, 80 (2023).
35. Hersbach, H. et al. ERA5 monthly averaged data on single levels from 1940 to present. Copernicus Climate Change Service (C3S) Climate Data Store (CDS), https://doi.org/10.24381/cds.f17050d7 (Accessed 10 December 2024).
36. Hersbach, H. et al. The ERA5 global reanalysis. *Q. J. R. Meteorol. Soc.* **146**, 1999–2049 (2020).
37. Yu, R. & Zhou, T. Impacts of winter NAO on March cooling trends over the subtropical Eurasian continent in the recent half century. *Geophys. Res. Lett.* **31**, L12 (2004).
38. Goosse, H. et al. Introduction to climate dynamics and climate modeling. https://www.climate.be/textbook/chapter5_node5.xml (2023).
39. Stenchikov, G. et al. Arctic Oscillation response to the 1991 Mount Pinatubo eruption: effects of volcanic aerosols and ozone depletion. *J. Geophys. Res.* **107**, 4803 (2002).
40. Trigo, R. M., Osborn, T. J. & Corte-Real, J. M. The North Atlantic Oscillation influence on Europe: climate impacts and associated physical mechanisms. *Clim. Res.* **20**, 9–17 (2002).
41. Hurrell, J. W. Decadal trends in the North Atlantic Oscillation: Regional temperatures and precipitation. *Science* **269**, 676–679 (1995).
42. Dogar, M. M. & Sato, T. Regional climate response of Middle Eastern, African, and South Asian monsoon regions to explosive volcanism and ENSO forcing. *J. Geophys. Res. Atmos.* **124**, 7580–7598 (2019).
43. Wegmann, M. et al. Volcanic influence on European summer precipitation through monsoons: possible cause for "Years without Summer". *J. Clim.* **27**, 3683–3691 (2014).
44. Willmott, C. J., & Matsuura, K. Terrestrial Air Temperature and Precipitation: Monthly and Annual Time Series (1950–1999). http://climate.geog.udel.edu (2001).
45. DallaSanta, K., Gerber, E. P. & Toohey, M. The circulation response to volcanic eruptions: the key roles of stratospheric warming and eddy interactions. *J. Clim.* **32**, 1101–1120 (2019).
46. Ineson, S. & Scaife, A. A. The role of the stratosphere in the European climate response to El Niño. *Nat. Geosci.* **2**, 32–36 (2009).
47. Jones, G. S., Gregory, J. M., Stott, P. A., Tett, S. F. B. & Thorpe, R. B. An AOGCM simulation of the climate response to a volcanic super-eruption. *Clim. Dyn.* **25**, 725–738 (2005).
48. Bittner, M., Schmidt, H., Timmreck, C. & Sienz, F. Using a large ensemble of simulations to assess the Northern Hemisphere stratospheric dynamical response to tropical volcanic eruptions and its uncertainty. *Geophys. Res. Lett.* **43**, 9324–9332 (2016).
49. Perlwitz, J. & Graf, H.-F. The statistical connection between tropospheric and stratospheric circulation of the Northern Hemisphere in winter. *J. Clim.* **8**, 2281–2295 (1995).
50. Xing, C. et al. Boreal winter surface air temperature responses to large tropical volcanic eruptions in CMIP5 models. *J. Clim.* **33**, 2407–2426 (2020).
51. Brown, F. et al. On the magnitude and sensitivity of the quasi-biennial oscillation response to a tropical volcanic eruption. *Atmos. Chem. Phys.* **23**, 5335–5353 (2023).

52. DallaSanta, K., Orbe, C., Rind, D., Nazarenko, L. & Jonas, J. Response of the Quasi-Biennial Oscillation to historical volcanic eruptions. *Geophys. Res. Lett.* **48**, e2021GL095412 (2021).
53. Tatebe, H. et al. Description and basic evaluation of simulated mean state, internal variability, and climate sensitivity in MIROC6. *Geosci. Model Dev.* **12**, 2727–2765 (2019).
54. Kataoka, T. et al. Seasonal to decadal predictions with MIROC6: Description and basic evaluation. *J. Adv. Model. Earth Syst.* **12**, e2019MS002035 (2020).
55. Beljaars, A. C., Brown, A. R. & Wood, N. A new parametrization of turbulent orographic form drag. *Q. J. R. Meteorol. Soc.* **130**, 1327–1347 (2004).
56. Sato, M., Hansen, J. E., McCormick, M. P. & Pollack, J. B. Stratospheric aerosol optical depths, 1850–1990. *J. Geophys. Res.* **98**, 994 (1993). D12, 22,987–22.
57. Lim, H. G. et al. Threshold of the volcanic forcing that leads the El Niño-like warming in the last millennium: results from the ERIK simulation. *Clim. Dyn.* **46**, 3725–3736 (2016).
58. Toohey, M. et al. Disproportionately strong climate forcing from extratropical explosive volcanic eruptions. *Nat. Geosci.* **12**, 100–107 (2019).
59. Nakajima, T., Tsukamoto, M., Tsushima, Y., Numaguti, A. & Kimura, T. Modeling of the radiative process in an atmospheric general circulation model. *Appl. Opt.* **39**, 4869–4878 (2000).
60. Sekiguchi, M. & Nakajima, T. A k-distribution-based radiation code and its computational optimization for an atmospheric general circulation model. *J. Quant. Spectrosc. Radiat. Transf.* **109**, 2779–2793 (2008).
61. Dogar, M. M., Sato, T. & Liu, F. Ocean Sensitivity to Periodic and Constant Volcanism Abstract. *Sci. Rep.* **10**, https://doi.org/10.1038/s41598-019-57027-0 (2020).

Acknowledgements
This research was supported by the MEXT Program for Advanced Studies of Climate Change Projection (SENTAN) under Grant Number JPMXD0722681344 and by the Japan Society for the Promotion of Science (JSPS) through a Grant-in-Aid for Scientific Research (Grant Numbers JP23K22574 and JP24K00700). The numerical experiments in this study were performed using the Earth Simulator at the Japan Agency for Marine-Earth Science and Technology. The authors gratefully acknowledge Prof. John Nielsen-Gammon (Department of Atmospheric Sciences, Texas A&M University) for his valuable feedback, which significantly improved the quality of this study.

Author contributions
Dogar, M.M., Fujiwara, M., and Watanabe, S. conceived and designed the project. Dogar, M.M. and Watanabe, S. processed and analyzed the data. Abid, M.A., Habeebullah, T.M., and Khan, B. contributed to the analysis and interpretation of the results. Dogar, M.M., Watanabe, S., and Fujiwara, M. wrote the initial draft of the manuscript. All authors reviewed, commented on, and contributed to the improvement of the final manuscript.

Competing interests
The authors declare no competing interests.

Additional information
Supplementary information The online version contains supplementary material available at https://doi.org/10.1038/s41612-025-01201-x.

Correspondence and requests for materials should be addressed to Muhammad Mubashar Dogar.